Seismic Loss Assessment of Residential Buildings in Karaj, Iran, By Considering Near-Source Effects Using Stochastic Finite-Fault Approach

Nazila Kheirkhah
University of Tehran
Erfan Firuzi (e.firuzi@iiees.ac.ir)
IIEES: International Institute of Earthquake Engineering and Seismology
Mohsen Kalantari
K N Toosi University of Technology Faculty of Mechanical Engineering
Reza Alikhanzadeh
IIEES: International Institute of Earthquake Engineering and Seismology

Research Article

Keywords: Finite-fault approach, Seismic Risk, Residential buildings, Near-source effects, Karaj, Iran

Posted Date: January 11th, 2023

DOI: https://doi.org/10.21203/rs.3.rs-2215534/v2

Abstract

This study provides the results of a study conducted to evaluate the seismic loss of residential buildings in Karaj, Iran, caused by the rupture of North Tehran Fault (7.1 Mw). One of the main concerns of seismic risk assessment in Karaj is proper considering the near-source effects of the NTF fault, which passes through the city. In the present study, the finite-fault approach with dynamic corner frequency was first employed to simulate the acceleration time histories. This is an appropriate approach to take into account the source, path effects, directivity and site condition on seismic waves. The results of seismic hazard showed that the PGA values vary between 0.15 to 0.55g, with maximum values nearby the NTF fault. Afterwards, a high-quality database of residential buildings consists of 26 building types was compiled. A set of compatible vulnerability curves were also employed. The results indicated that the loss ratio, defined as the ratio of the loss to the total exposed economic value, for the whole of Karaj is about 18.2%±5.3. The northern parts of the city, which are close to the NTF fault, are the most vulnerable. A disaggregation analysis was also performed to identify the most vulnerable building types. The results showed that the adobe and low-quality masonry buildings contribute the most to loss. The findings from this study can be used by local authorities and managers to provide appropriate emergency and risk reduction plans in Karaj in the case of the NTF fault seismic scenario.

1. Introduction

Karaj is the capital of Alborz province, which is located in north of Iran. According to the most recent Statistical Center of Iran (SCI) data from 2016, total population of Karaj is about 1.97 million people. This metropolis, which is the fourth most populous city, has the highest population density of any Iranian city (SCI, 2016). Karaj also contributes more than 3% of the country's GDP (Gross Domestic Product) and is ranked 10th among Iran's provinces. In addition, Karaj is the most important city in close proximity to Tehran, Iran's capital, and can play a crucial role in responding to a natural disaster in Tehran. As a result, the safety of Karaj against natural hazards is of great importance to the government.

One of the most serious potential natural disaster threats in Karaj is earthquake. Tectonically, the city lies at the southern side of the Alborz Mountain, which is characterized by shallow large earthquakes (Berberian and Yeats, 1999). The North-Tehran Fault (NTF), Mosha, Eshtehard, and Taleghan are major active faults in this region (Ashtari et al., 2005). Figure 1 depicts Karaj border in relation to active faults. The NTF fault with the length of 110 Km is the closest fault to Karaj which crossing the northern parts of the city. Thus, it is considered as the most vulnerable seismic scenario in Karaj. This issue is also reflected in the study done by Jarahi (2016). He conducted a disaggregation analysis in Karaj, and the results indicated that the NTF, particularly in short periods, contributes the most to the seismic hazard of Karaj in return periods of 475 and 50 years. Ritz et al. (2012) indicated, based on past seismicity in the region, that the NTF might be the source of major earthquakes in Karaj. The occurrence of a strong earthquake is likely to result in numerous casualties, severe structural damages, and significant economic losses. This issue highlights the importance of conducting detailed risk assessments to address the impact of the NTF fault seismic scenario on the region. Such studies can play a crucial role in developing

appropriate risk reduction and emergency response plans to deal with the consequences of a major earthquake.

While the seismic hazard of Karaj has been assessed in a few studies, there is no study in the literature that evaluates the seismic risk in Karaj. Jarahi (2016) conducted a classical PSHA in Karaj to determine dominant earthquakes at the design-basis earthquake level, which corresponded to a 10% likelihood of occurrence in 50 years. He used the EZ-FRISK tool to perform the analysis, which consists of a logic tree with 120 branches. Jarahi (2016) reported a Peak Ground Acceleration (PGA) range of 0.45-0.60g on bed-rock in Karaj, which is significantly higher than the suggested value by the national Iranian building code, 0.35g (Standard 2800). According to Jarahi (2016) disaggregation analysis, the NTF has the highest contribution at the design-basis earthquake level. Jalalalhosseini et al (2018) carried out a time-dependent seismic hazard analysis for Tehran and surrounding area. They employed a model of smooth seismicity. They reported that the PGA value in Karaj is between 0.35 and 0.42g in return period of 475-years. In their study for evaluating risk adjusted maps for Karaj, Zaman and Ghayamghamian (2021) performed a classical PSHA. They used eight Ground Motion Prediction Equations (GMPEs) and one seismic source model. Their results showed a range of 0.3-0.45g for PGA on bed-rock in return period of 475-years.

Although the above studies provide information regarding seismic hazard in Karaj, they do not address the consequences of a vulnerable seismic scenario in Karaj. In addition, the near-source effects such as pulse waves and directivity, which are important issues in Karaj are not considered in their analysis. In fact, previous studies used GMPEs for quantifying the ground motion values. However, due to the lack of near-source strong ground motion data the empirical GMPEs are associated with uncertainties (Yu et al, 2022). GMPEs generally perform well in intermediate distance range (i.e., 10–100 Km) (Sorensen and Lang, 2015). The near-source ground motion values are substantially varied by factors like slip distribution, rupture directivity, and fault characteristics. To address the aforementioned technological gap, this study applied the stochastic finite-fault approach to provide ground motion shaking map in Karaj for the NTF seismic scenario. This is an appropriate approach for modeling the entire ground motion propagation process by considering the source, path and site condition. The outcome of seismic hazard analysis is also used to assess the possible losses to Karaj's residential buildings.

The primary purpose of this study is to quantify the seismic risk of Karaj in terms of losses of residential buildings using an approach that properly accounts for near-source effects. To do so, the ground motion shaking map of Karaj from the rupture of the NTF is first derived using the stochastic finite-fault approach. Then, the procedure of compiling the building exposure model and selecting appropriate fragility/vulnerability curves are introduced. Next, the results of losses to the residential buildings is presented. Finally, a comprehensive discussion regarding the results and uncertainties are provided.

2. The Ground Motion Shaking Map Of Karaj From The Rupture Of Ntf Fault

There are a number of approaches in literature for simulating the ground motion time histories from a near seismic source, which are categorized into three main groups: 1) Physics-based approaches, 2) Stochastic methods, and 3) Hybrid approaches. A summary review of them with their main features can be found in the study of Douglas and Aochi (2008). In the present study, the stochastic finite-fault approach with dynamic corner frequency developed by Motazedian and Atkinson (2005) is employed. This approach integrates the characteristics of the earthquake source, path, directivity and site effects through a statistical approach. This method has an appropriate computation efficiency and widely used in simulating the ground motion waveforms in areas where past earthquake data is scarce. Figure 2 shows a general analytical framework of the stochastic finite-fault method. As depicted, in the first step, the rupture area is divided into sub-faults which are considered as point sources. In the second step, the ground motion waveform of sub-faults is derived. Finally, the ground motion from the rupture of the whole of fault is obtained by superimposing the waveform of sub-faults with an appropriate time delay. Equation (1) is a mathematical representation of above explanations.

$$a(t) = \sum_{i=1}^{nl} \sum_{j=1}^{nw} a_{ij}(t + \Delta_{ij}) \qquad (1)$$

In the above equation, nl and nw represent the number of sub-faults along the strike and dip of the fault, respectively. The acceleration time history from each element is denoted by aij and △ij is the delay time which is a function of the distance between the source and observation point.

The waveform of sub-faults are derived from the approach proposed by Motazedian and Atkinson (2005). The middle box of Figure 2 shows a schematic analytical flow of this approach. As depicted, a Gaussian white noise signal is first generated. This is multiplied by a time window function. Generally, the time window function proposed by Saragoni-Hart is used in the simulation due to its appropriate representation of the average envelope of the squared acceleration time series. It is not, however, the ideal shape for earthquakes with two or more consecutive ruptures (Zhou and Chang, 2019). Then, the normalized Fourier spectrum of the time window signal is multiplied by the source amplitude in frequency domain. The source spectrum amplitude comes from the integration of source, path and site response. Finally, the simulated ground motion waveform is obtained by converting the signal to the time domain.

The mathematical form of Fourier amplitude of sub-fault is presented in equation (2). A detailed description of parameters in the following equation is presented in Table 1.

$$A_{ij}(f) = CH_{ij}M_{0ij}\frac{(2\pi f)^2}{1+\left(\frac{f}{f_{0ij}}\right)^2}e^{-\pi f k_0}\frac{e^{-\frac{\pi f R_{ij}}{Q(f)\beta}}}{R_{ij}}G(R_{ij}) \qquad (2)$$

Proper calibration of influencing factors such as source, rupture area, path and site parameters is an important step in stochastic finite-fault approach. Due to the absent of instrumentally records on the NTF, parameters are taken from literature. As illustrated in Figure 3, the NTF seismic scenario has an approximate length of 110 Km with two main segments (Berberian et al, 1983). Here, the western segment, which is closer to Karaj, is considered as worst-case seismic scenario. Based on the empirical relation of Wells and Coppersmith (1994), the western segment with an approximate length of 57 Km has the potential of producing an earthquake with magnitude of 7.1 (Mw). This moment magnitude corresponds to a rupture plane with length of 46 and 26 Km along the fault's strike and dip, respectively. The fault plane is schematically depicted in Figure 3. According to Samaie et al (2012) the strike and dip of the NTF fault are 305^{o} and 35^{o}, respectively. Because there are no instrumental strong earthquake data on the NTF, providing an accurate estimation of stress drop is associated with uncertainties. In this study, the value of stress drop is fixed to 50 bar, as proposed by Zafarani et al (2009). The quality factor in the present study is also taken from the study of Zafarani et al (2009). They proposed the form of for earthquakes in the north of Iran. This value is derived from the Manjil-Roudbar earthquake (7.4 Mw, 1990). Similarly, Motazedian (2006) developed a trilinear geometric spreading function based on data from the Manjil-Roudbar earthquake. Here, the same model is used. The proportion of pulsing area is assumed to be 50%, implying that during sub-fault rupture, no more than 50% of all sub-faults can be active, while the remainder are passive. Matazedina and Atkinson (2005) proposed this value based on the concept of self-healing provided by Heaton (1990). As there is no information on the slip distribution, a random normally slip distribution is employed for analysis.

In the present study, the analysis is carried out using the EXSIM code written in FORTRAN (Motazedian and Atkinson, 2005). The analysis is performed in a 0.5x0.5 Km grid cell. Figure 4 shows the results based on the above parameters on the bed-rock within Karaj's 12 municipal districts. As shown, the PGA values range from 0.1 to 0.42g, with the highest values in the north of Karaj nearby the NTF fault. Figure 5 presents the simulated time history waveform in 5 locations of Karaj (yellow triangle in Figure 4). As shown, time history waveform of points in the north of Karaj has greater amplitude; while, time history waveform of points in the south of Karaj (which are far from NTF fault) has a weaker amplitude. This is in accordance with our expectations. Figure 5 also shows the pseudo response acceleration for the same points. Similarly, points located in north of Karaj has higher pseudo response acceleration.

To obtained the soil surface acceleration the V_{S30} map of region is required. The V_{S30} map is extracted from a microzonation study done by International Institute of Earthquake Engineering and Seismology (IIEES, 2013). Figure 6 shows the V_{S30} map of Karaj. As depicted, the northern part of the city, near the foothill of Alborz Mountains, has higher V_{S30}; while, the southern part of the city has lower V_{S30}. Figure 7 shows distribution of PGA values on the soil. As depicted, by employing the local site condition, the acceleration in the southern and central parts of the city is increased (i.e., district number 1, 2, 4 and 7). The existence of soft soil in these regions is the primary cause of such amplification.

To compare the results with GMPEs, a deterministic analysis is performed using the open-source OpenQuake program (Pagani et al, 2014). The epistemic uncertainty of GMPEs is considered in analysis

using logic tree. To do so, five NGA-west2 relations with equal weights are applied (Bozorgnia et al, 2014). Figure 8 shows distribution of PGA on the soil surface for the same seismic scenario. As depicted, there is appropriate consistency between the values of stochastic finite-fault model and GMPEs. Figure 9 shows a grid-by-grid comparison of results from GMPEs and simulation. As depicted, the PGA values from the stochastic finite-fault are slightly higher in short distances; while, in far distances the finite-fault approach shows lower acceleration in relation to GMPEs.

3. Compiling Exposure Model And Selecting Appropriate Vulnerability Curves

Compiling a reliable database of building stock and exposed population is an important component in seismic risk assessment. Due to computation efficiency, in urban seismic risk assessment, buildings are generally categorized in groups which show similar performance in different levels of ground motions. Silva et al (2022) provides a short review of available building classification in literature. Due to the lack of detailed information about building characteristics, application of them in regions like Iran is not practical. As a case in point, the HAZUS building classification focuses on structural aspects of building; while, information about the seismic load resistance system of buildings is not available in Iran. Therefore, the majority of seismic risk assessments in Iran are performed by taking generic building characteristics into account. On the one hand, this issue introduces uncertainties on results. On the other hand, employing a set of unrealistic assumptions for building classification imposes greater uncertainty on the outcomes.

In the course of this study, the information supplied by Statistical Center of Iran (SCI) is used for compiling the building exposure model. This is the official agency for collecting demographic and building data in Iran. SCI provides information about buildings construction materials and ages. Buildings are classified into four groups by SCI depending on their construction materials: concrete, steel, masonry, and adobe. The seismic regulation employed in the design of structures in Iran is inferred by the year of construction. The Iranian Code of Practice for Seismic Resistant Design of Building (Standard No. 2800) is the primary reference for seismic design of structures. Building and Housing Research Center (BHRC) has currently published four versions of this standard. Buildings constructed prior to 1987 are designed by first edition and considered as the low-code. Structures constructed within time interval of 1987 to 1996 are designed by the second edition and considered as the mid-code. Buildings constructed after 2005 are designed in accordance with the third and fourth editions of Standard No. 2800. Thus, they are classified as high-code. In addition, buildings based on their height are categorized in three groups: low-rise (1-3 floors), mid-rise (4-6 floors) and high-rise (more than 7 floors). Accordingly, 26 building types based on above factors are considered in the present study. A summary of building taxonomy is provided in Table 2.

Figure 10 shows the number of buildings with different construction material and construction years. The vast majority of buildings, as depicted, are mid-quality steel and masonry structures. The distribution of different building types within 12 municipal districts of Karaj is shown in Figure 11. As depicted, the

highest building density are in the southern parts of the city. However, most of low-quality structures are located in the north of Karaj near the NTF fault.

In addition to building inventories, a set of compatible fragility or vulnerability curves is required. There are a number of local fragility/vulnerability curves for typical residential buildings in Iran. The most recent are sturdies of Fallah Tafti et al. (2020) and Bastami et al (2022). Fallah Tafti et al. (2020) developed fragility curves for 19 building classes in Iran by compiling a set of existing fragility curves and merging them using the Analytic Hierarchy Approach (AHP). Bastami et al (2022) by considering construction material, age, and building's height provided a set of 26 vulnerability curves for residential buildings in Iran. They also validated their model based on Iran's past earthquakes data. In the present study, the vulnerability curves proposed by Bastami et al (2022) are used due to its compatibility with pre-defined building classes. Figure 12 shows the vulnerability curves provided by Bastami et al (2022). As depicted, masonry, adobe and wood are the most vulnerable building classes.

4. Seismic Risk Assessment Of Karaj

This section provides the seismic risk of Karaj in terms of residential buildings losses. The analysis is performed using the census blocks from SCI, which is the highest available geographic resolution data. Figure 13 shows the distribution of census blocks within Karaj. In this study, the census block data are first mapped in grid cells of 200x200 meters and then the seismic loss of residential buildings are performed. This is in accordance of geographic resolution f V_{S30} information. Bal et al (2010) evaluated the impact of the spatial resolution of the exposure model on losses. Their results demonstrated that the aggregated losses in an urban area, in terms of mean damage ratio (MDR), is relatively insensitive to the geographical resolution of the exposure model. Thus, a grid ell of 200x200 meters which provides appropriate computation efficiency and compatible with size of most of census blocks are used.

Proper capturing of uncertainties is an important step of seismic risk assessment. There are two main sources of variability: 1) uncertainties regarding ground motion values, and 2) uncertainties of vulnerability curves.

Uncertainties of ground motion values are generally expressed in terms of inter-event and intra-event variabilities. The former comes from variabilities from one earthquake to another; while the latter stems from one location to another (Silva 2018). Due to fact that the ground motion values in the present study is estimated from a specific seismic scenario, all variability of ground motion values can be considered from the intra-event type. Figure 14 shows the variability of PGA values derived from stochastic finite-fault in grid cells. The circles are PGA values derived from simulation and red solid and blue dashed lines are mean and intra-event variability, respectively. Here, for considering the intra-event variability, 100,000 ground motion shaking maps by random sampling of intra-event variabilities is generated. The random sampling is performed by taking into account the spatial correlation caused by coherent of source, path and site wave propagation (Verros et al, 2017). The impact of spatial correlation on seismic loss

estimation is demonstrated in several studies (Weatherill et al, 2015; Firuzi et al, 2019). In the present study, the spatial correlation model proposed by Zafarani et al (2022) is applied.

Similarly, the variability of vulnerability curves is considered in analysis using the random sampling. In this procedure, for each ground motion values 10 loss ratios from a normal distribution by considering the mean and standard deviation of vulnerability curves is sampled. A sample of loss map in terms of mean loss ratio, which is defined as the loss value to the total economic value, is presented in Fig. 15. As depicted, the highest losses are experienced in northern districts of Karaj (for example, districts number 1, 2 and 11) which are nearby the NTF fault. Thus, it is important to local authorities and people in charge of emergency response provide appropriate emergency and disaster risk plans in these regions. The mean value of loss ratio for the whole of Karaj is about 18.2%±5.3 (the variability is derived from 100,000 ground motion shaking maps). This means that in the case of NTF 18.2 percent of total economic values of buildings in Karaj should be invested for reconstruction.

To identify building types with high contribution in losses, a disaggregation analysis per building classes is performed. The results are presented in Fig. 16. As depicted, the low-code masonry and adobe building classes contribute the most in seismic vulnerability of Karaj. These building classes are generally the home of the low-income people. Thus, this is important for local authorities to provide appropriate plans for strengthening such kinds of buildings. This can be accomplished by providing incentives such as low-interest loans to encourage individuals to renovate their structures.

It should be mentioned that the analysis carried out in the present study can be significantly improved by employing analytical approaches like capacity spectrum methods. In this approach, the loss of a building type is determined through combination of response spectrum and the capacity curve accounts for non-linear behavior of buildings. However, such analysis requires detailed building information which are not accessible. By considering the above challenges, the outcomes of this study provide a first insight for local authorities and people in charge of seismic risk reduction plans in Karaj in the case of NTF rupture.

5. Conclusion

This study presents the results of a study carried out to evaluates the seismic risk, in terms of losses to the residential buildings, in Karaj, Iran in the case of the rupture of NTF fault. The main motivation of the authors for the present study is applying an improved approach to consider the near-source effects from the NTF fault which passes through the city. In this study, the finite-fault with dynamic corner frequency approach is applied for simulating the time history acceleration waveforms. This is an appropriate approach for describing the rupture of source more realistically, and taking factors such as the path and site condition of seismic waves into account.

The study is performed for the western segment of the NTF fault, which is capable to produce an earthquake with moment magnitude of 7.1 (Mw). This seismic scenario corresponded to 46 and 26 Km of rupture along the strike and dip of the NTF fault, respectively. The results indicated that the PGA for this seismic scenario varied between 0.15 to 0.55g, with maximum values in the northern parts of the city

near the NTF fault. The results were also compared to NGA-West2 relations. Although, there is appropriate consistency between the ground motion values of GMPEs and simulation approach; the finite-fault approach presents the higher PGA values in close proximity to the NTF fault.

The outcomes of seismic hazard analysis is used to assess the potential losses to residential buildings in Karaj. To do so, a high-quality database of residential buildings in Karaj is compiled. Buildings are classified in groups according to factors such as construction material, age and height. The final exposure model composed of 26 building classes. The vulnerability curves developed by Bastami et al (2022) are also employed for seismic loss evaluation. It should be noted that the building taxonomy used by Bastami et al (2022) is in accordance with pre-defined building classes. The aleatory uncertainty of ground motion values incorporated in analysis using the random sampling of intra-event variability based on spatial correlation. The results indicated that the loss ratio for the whole of Karaj is about 18.2%±5.3. The highest vulnerability occurred in the northern parts of the city (districts number 1, 2 and 11), near the NTF fault. In addition, a disaggregation analysis is performed to identify the most vulnerable building classes. The results showed that the low-quality masonry and adobe have the highest contribution to the losses of Karaj. These building types are generally the home of low-income people. Thus, government should provide appropriate plans to decrease the seismic risk in such building types.

It should be mentioned that the results of this study can be significantly enhanced by providing appropriate adjustment in parameters of ground motion simulation and detailed building information. Such information enables us to employ analytical approach such as response spectrum methods. Despite aforementioned challenges, results of this study provide appropriate insights for local disaster management authorities to provide necessary emergency-response and preparedness plans.

Statement And Declarations

a. Ethics approval

The authors consciously assure that this material is the authors' own original work, which has not been previously published elsewhere.

b. Consent to participate

The authors consciously assure that in this manuscript the following is fulfilled:

1) This material is the authors' own original work, which has not been previously published elsewhere.

2) The paper is not currently being considered for publication elsewhere.

3) The paper reflects the authors' own research and analysis in a truthful and complete manner.

4) The paper properly credits the meaningful contributions of co-authors and co-researchers.

5) The results are appropriately placed in the context of prior and existing research.

6) All sources used are properly disclosed (correct citation).

7) All authors have been personally and actively involved in substantial work leading to the paper, and will take public responsibility for its content.

The authors agree with the above statements and declare that this submission follows the policies of Committee on Publication Ethics (COPE) as outlined in the Guide for Authors and in the Ethical Statement.

c. Availability of data and material

The most important data used in the present study is earthquake catalog which is available on public domain of https://irsc.ut.ac.ir

d. Competing Interests

The authors have no relevant financial or non-financial interests to disclose.

e. Funding

The authors declare that no funds, grants, or other support were received during the preparation of this manuscript.

f. Author's Contributions

All authors contributed to the study conception and design. Material preparation, data collection and analysis were performed by all authors. The first draft of the manuscript was written by Erfan Firuzi and the other authors commented on manuscript. All authors read and approved the final manuscript.

g. Acknowledgment

The authors gratefully appreciate all those individuals and organizations contributing to the compiling data sets used in the present study, particularly the International Institute of Earthquake Engineering and Seismology (IIEES) for providing the VS30 map of Karaj.

References

1. Ashtari, M., Hatzfeld, D., & Kamalian, N. (2005). Microseismicity in the region of Tehran. Tectonophysics, 395(3-4), 193-208.
2. Berberian, M., & Yeats, R. S. (1999). Patterns of historical earthquake rupture in the Iranian Plateau. Bulletin of the Seismological society of America, 89(1), 120-139.
3. Jalalalhosseini, S. M., Zafarani, H., & Zare, M. (2018). Time-dependent seismic hazard analysis for the Greater Tehran and surrounding areas. Journal of Seismology, 22(1), 187-215.

4. Jarahi, H. (2016). Probabilistic seismic hazard deaggregation for Karaj City (Iran). Am. J. Eng. Applied Sci, 9, 520-529.
5. Statistical Centre of Iran (SCI), 1956–2015, Statistical Centre of Iran, Vice-Presidency for Strategic Planning and Supervision, Tehran, National Census of Population and Housing Techical Reports, Sarshomāri 2016 (1395), 2011 (1390), 2006 (1385), 1996 (1375), 1986 (1365), and 1976 (1355): Tehran, SCI, formerly, the Plan & Budget Organization of the Imperial Government of Iran, Statistical Centre, http://www.amar.org.ir/Default.aspx?tabid=116 (accessed 2018).
6. Zaman, M., & Ghayamghamian, M. R. (2021). Risk-adjusted Design Basis Earthquake's Adequacy for use in Seismic Design Codes.
7. IIEES (International Institute of Earthquake Engineering and Seismology) (2013). The Micro-zonation study of Karaj (in persian)
8. Ritz, J. F., Nazari, H., Balescu, S., Lamothe, M., Salamati, R., Ghassemi, A., ... & Saidi, A. (2012). Paleoearthquakes of the past 30,000 years along the North Tehran Fault (Iran). Journal of Geophysical Research: Solid Earth, 117(B6).
9. Douglas, J., & Aochi, H. (2008). A survey of techniques for predicting earthquake ground motions for engineering purposes. Surveys in geophysics, 29(3), 187-220.
10. Zhou, H., & Chang, Y. (2019). Stochastic finite-fault method controlled by the fault rupture process and its application to the Ms 7.0 Lushan Earthquake. Soil Dynamics and Earthquake Engineering, 126, 105782.
11. Motazedian D, Atkinson GM (2005) Stochastic finite-fault modeling based on a dynamic corner frequency. Bull Seismol Soc Am 95: 995–1010.
12. Silva, V., Brzev, S., Scawthorn, C., Yepes, C., Dabbeek, J., & Crowley, H. (2022). A building classification system for multi-hazard risk assessment. International Journal of Disaster Risk Science, 13(2), 161-177.
13. Sørensen, M. B., & Lang, D. H. (2015). Incorporating simulated ground motion in seismic risk assessment: Application to the Lower Indian Himalayas. Earthquake Spectra, 31(1), 71-95.
14. Building & Housing Research Center, "Iranian Code of Practice for Seismic Resistant Design of Buildings - Standard No. 2800 – 3rd Revision," Tehran, Iran, 2005.
15. Yu, R., Song, Y., Guo, X., Yang, Q., He, X., & Yu, Y. (2022). Seismic hazard analysis for engineering sites based on the stochastic finite-fault method. Earthquake Science, 35(5), 314-328.
16. Wells, D. L., & Coppersmith, K. J. (1994). New empirical relationships among magnitude, rupture length, rupture width, rupture area, and surface displacement. Bulletin of the seismological Society of America, 84(4), 974-1002.
17. Samaei, M., Miyajima, M., Saffari, H., & Tsurugi, M. (2012). Finite fault modeling of future large earthquake from north Tehran fault in Karaj, Iran. Journal of Japan Society of Civil Engineers, Ser. A1 (Structural Engineering & Earthquake Engineering (SE/EE)), 68(4), I_20-I_30.
18. Motazedian, D. (2006). Region-specific key seismic parameters for earthquakes in northern Iran. Bulletin of the Seismological Society of America, 96(4A), 1383-1395.

19. Heaton, T. H. (1990). Evidence for and implications of self-healing pulses of slip in earthquake rupture. Physics of the Earth and Planetary Interiors, 64(1), 1-20.
20. Zafarani, H., Noorzad, A., Ansari, A., & Bargi, K. (2009). Stochastic modeling of Iranian earthquakes and estimation of ground motion for future earthquakes in Greater Tehran. Soil Dynamics and Earthquake Engineering, 29(4), 722-741.
21. Pagani, M., Monelli, D., Weatherill, G., Danciu, L., Crowley, H., Silva, V., ... & Vigano, D. (2014). OpenQuake engine: An open hazard (and risk) software for the global earthquake model. Seismological Research Letters, 85(3), 692-702.
22. Bozorgnia, Y., Abrahamson, N. A., Atik, L. A., Ancheta, T. D., Atkinson, G. M., Baker, J. W., ... & Youngs, R. (2014). NGA-West2 research project. Earthquake Spectra, 30(3), 973-987.
23. Fallah Tafti, M., Amini Hosseini, K., & Mansouri, B. (2020). Generation of new fragility curves for common types of buildings in Iran. Bulletin of Earthquake Engineering, 18(7), 3079-3099.
24. Bastami, M., Abbasnejadfard, M., Motamed, H., Ansari, A., & Garakaninezhad, A. (2022). Development of hybrid earthquake vulnerability functions for typical residential buildings in Iran. International Journal of Disaster Risk Reduction, 103087.
25. Bal, I. E., Bommer, J. J., Stafford, P. J., Crowley, H., & Pinho, R. (2010). The influence of geographical resolution of urban exposure data in an earthquake loss model for Istanbul. Earthquake Spectra, 26(3), 619-634.
26. Silva, V. (2018). Critical issues on probabilistic earthquake loss assessment. Journal of Earthquake Engineering, 22(9), 1683-1709.
27. Verros SA, Wald DJ, Worden CB, Hearne M, Ganesh M (2017) Computing spatial correlation of ground motion intensities for shakemap. Computers and Geosciences 99:145-154
28. Weatherill, G. A., Silva, V., Crowley, H., & Bazzurro, P. (2015). Exploring the impact of spatial correlations and uncertainties for portfolio analysis in probabilistic seismic loss estimation. Bulletin of Earthquake Engineering, 13(4), 957-981.
29. Firuzi, E., Ansari, A., Amini Hosseini, K., & Rashidabadi, M. (2019). Probabilistic earthquake loss model for residential buildings in Tehran, Iran to quantify annualized earthquake loss. Bulletin of earthquake engineering, 17(5), 2383-2406.
30. Zafarani, H., Ghafoori, S. M. M., & Adlaparvar, M. R. (2022). Spatial correlation of peak ground motions and pseudo spectral acceleration based on the Iranian multievent datasets. Journal of Earthquake Engineering, 26(12), 6042-6062.

Tables

Tables 1 to 2 are available in the Supplementary Files section

Figures

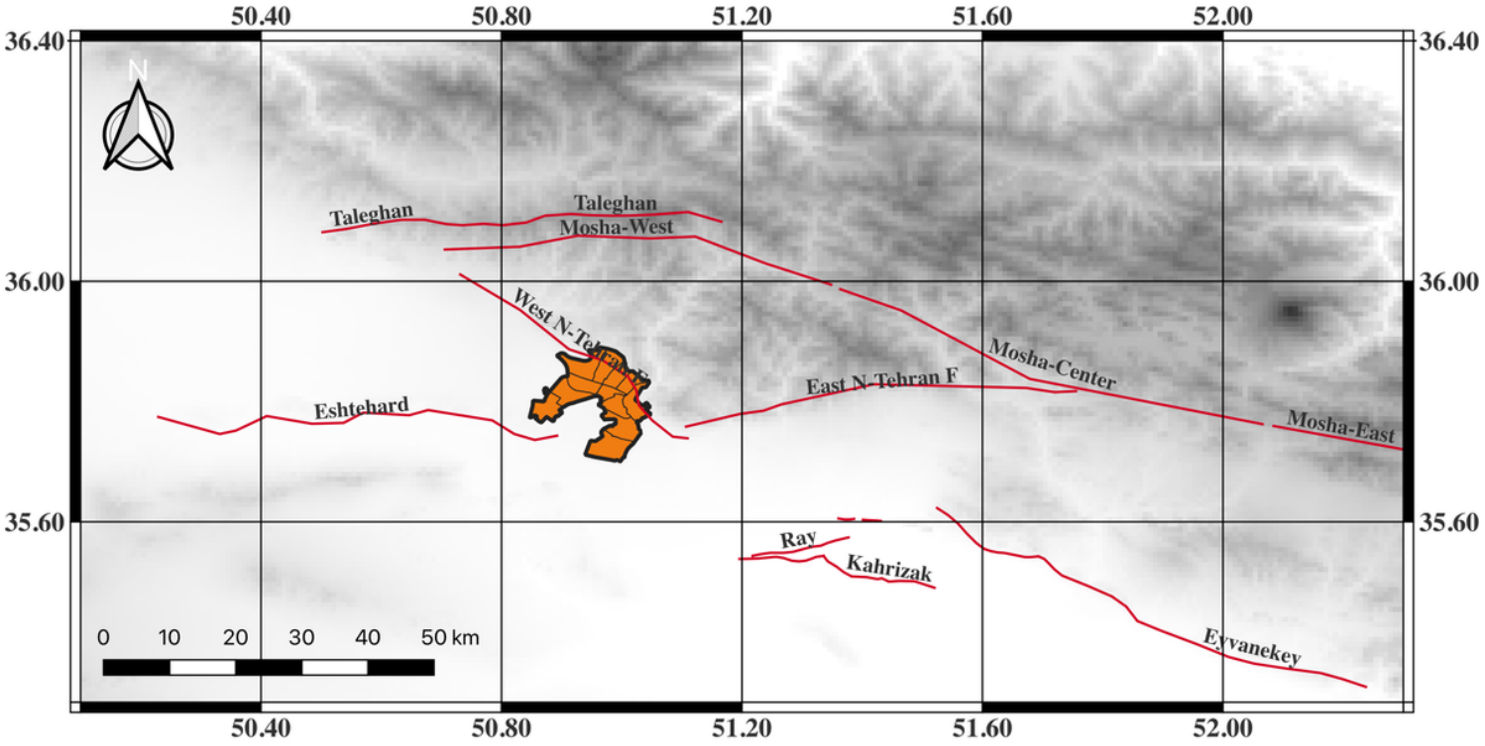

Figure 1

Distribution of major active faults in relation to Karaj border (the western segment of N-Tehran fault passes through Karaj)

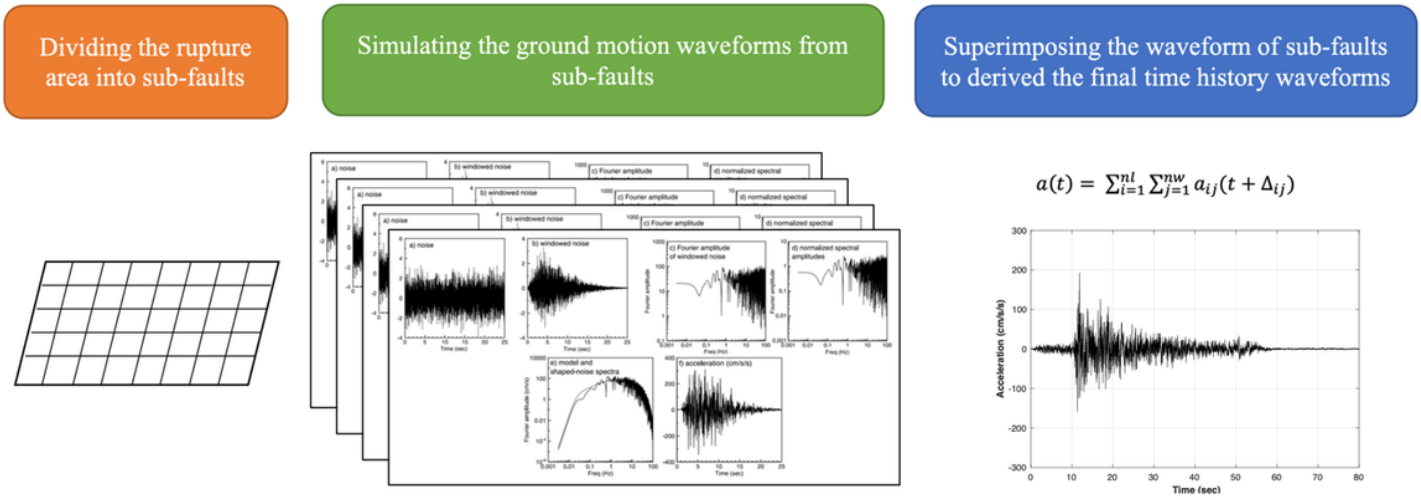

Figure 2

A schematic analytical flow of deriving the ground motion time histories using the stochastic finite-fault method (figure reproduced from study of Zhou and Chang (2019))

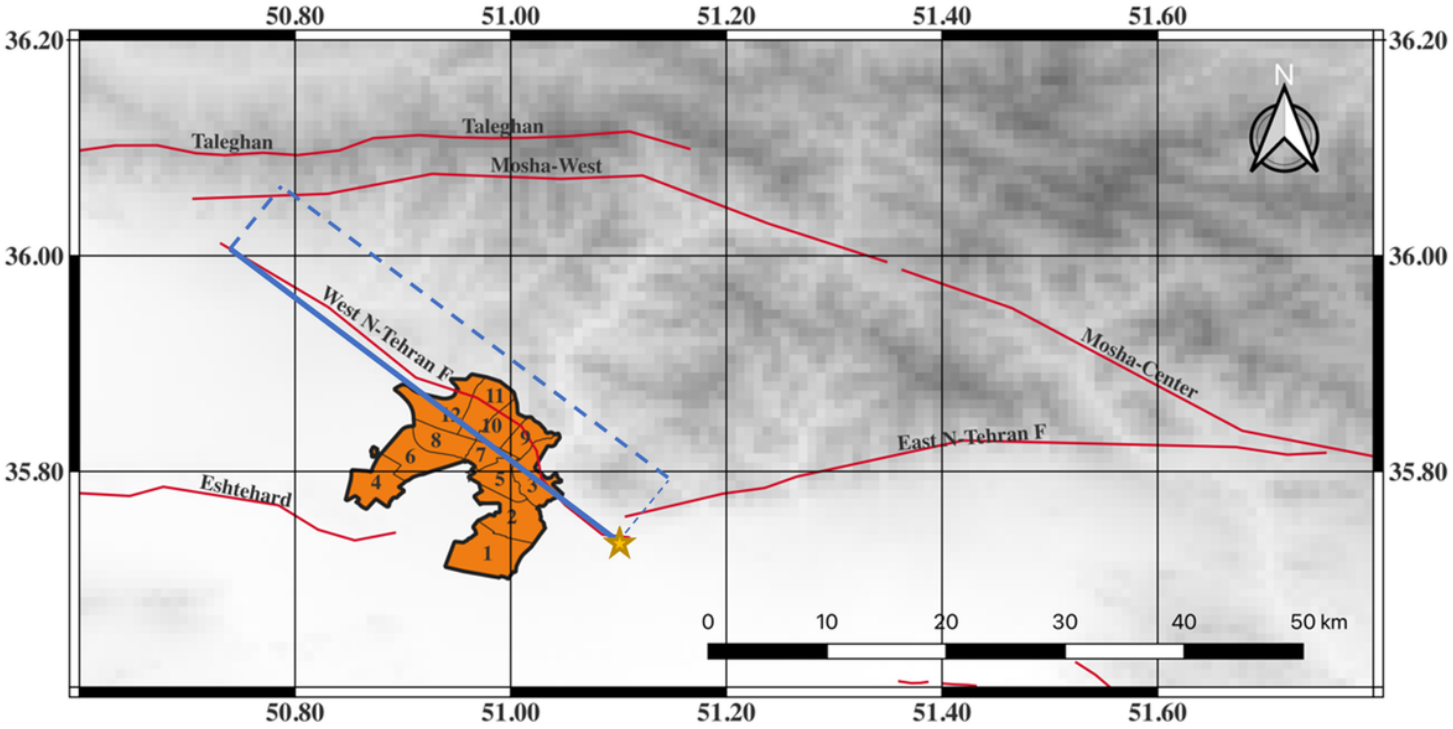

Figure 3

The location of two main segments of NTF in relation to Karaj boundaries (solid blue line is upper edge; dash blue line are lower edge trace and yellow star is upper edge point)

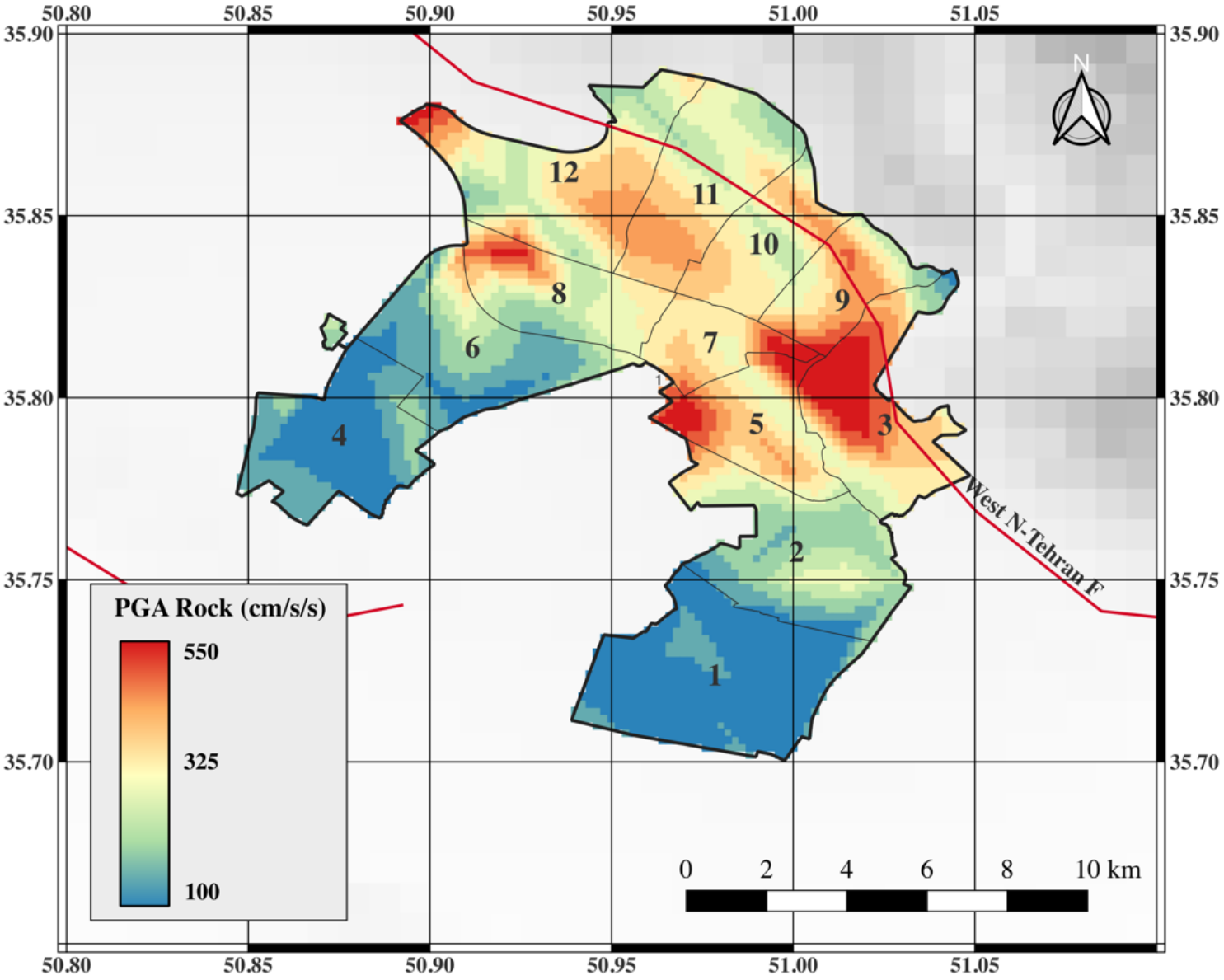

Figure 4

Distribution of PGA values on the bed-rock within 12 municipal districts of Karaj; yellow triangles are locations in Karaj which their time history waveforms are depicted as sample

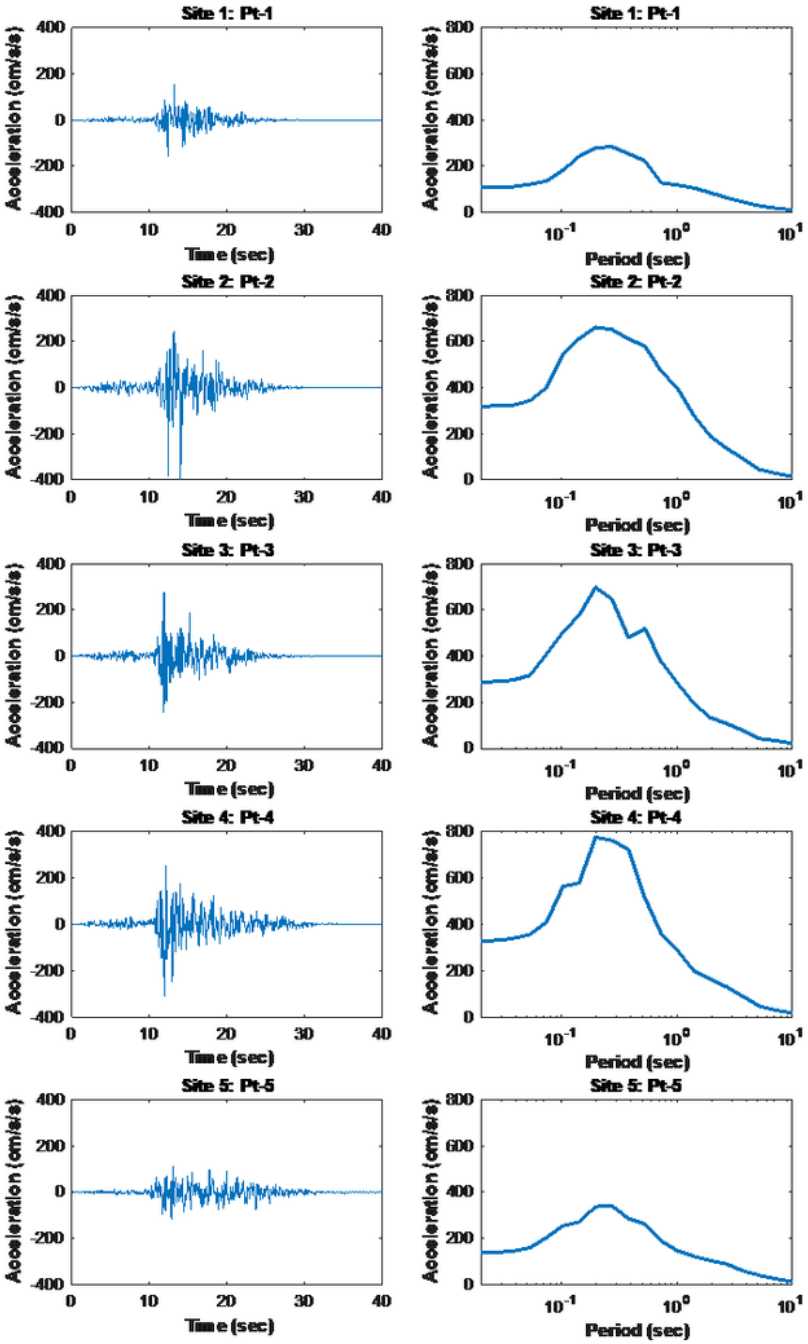

Figure 5

The time history waveform and their corresponding Pseudo response acceleration in five points (depicted in Figure 4 by yellow triangles) in Karaj

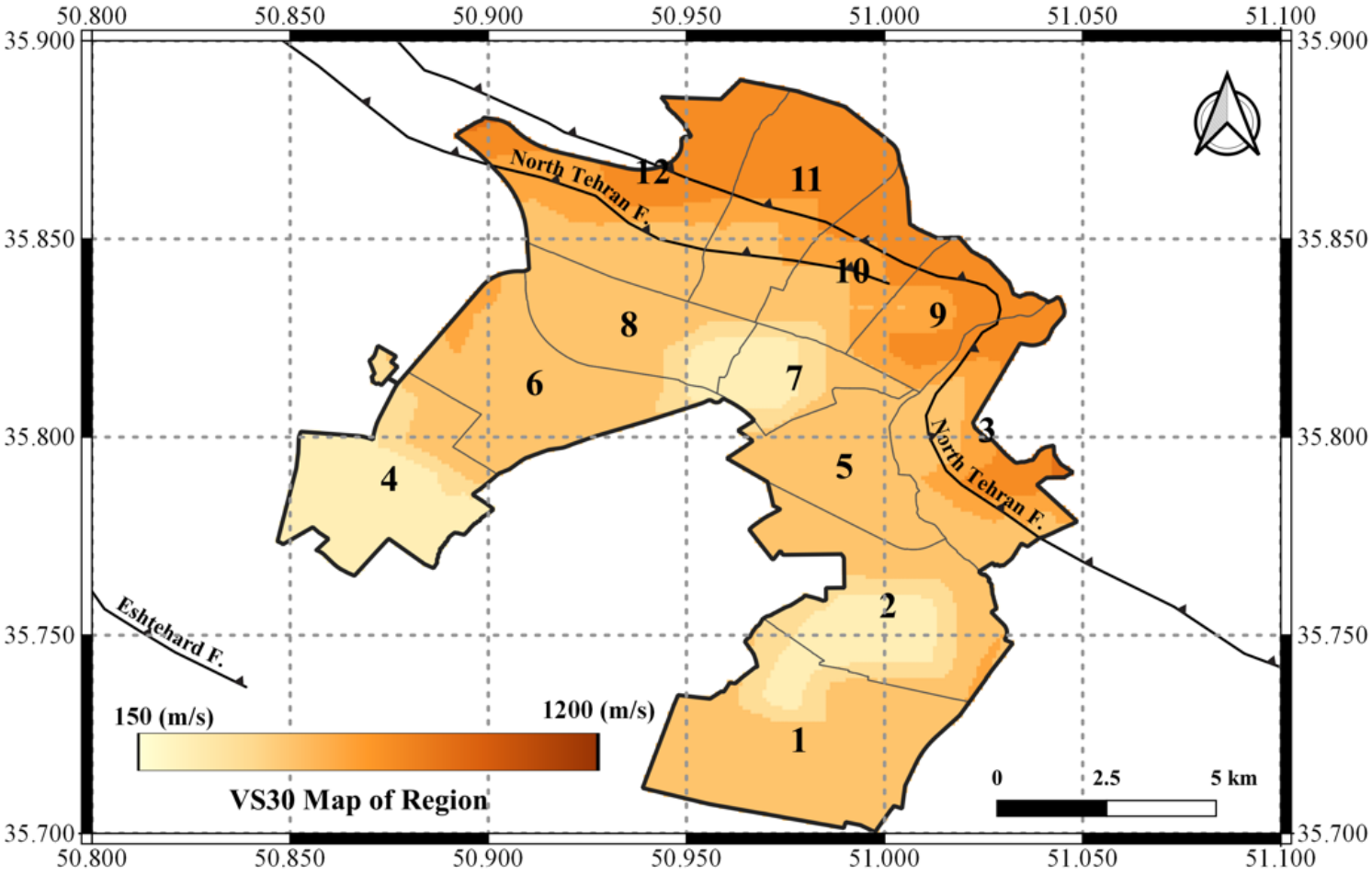

Figure 6

V_{S30} map of Karaj (data are from IIEES, 2013)

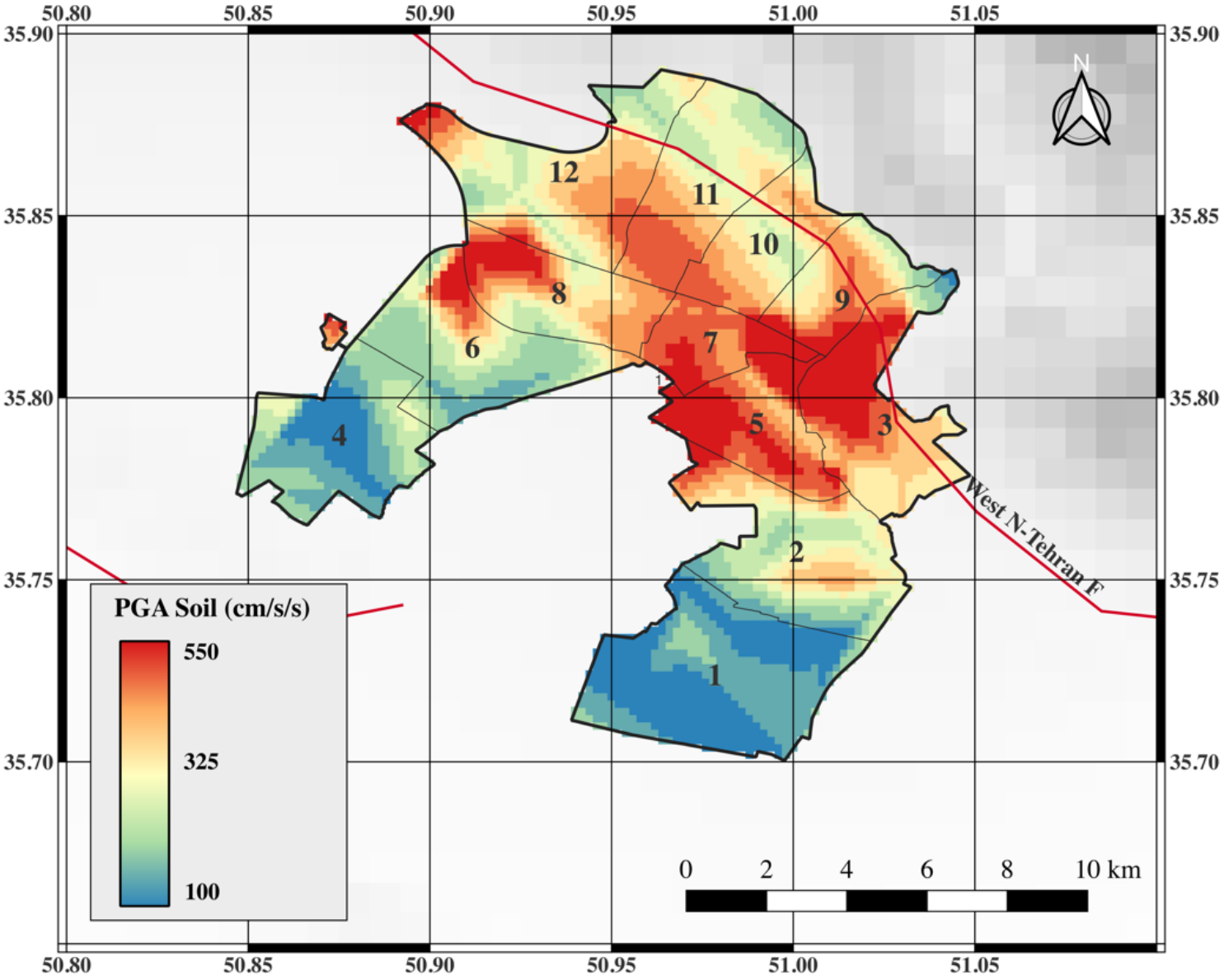

Figure 7

Distribution of PGA values on the soil surface within 12 municipal districts of Karaj

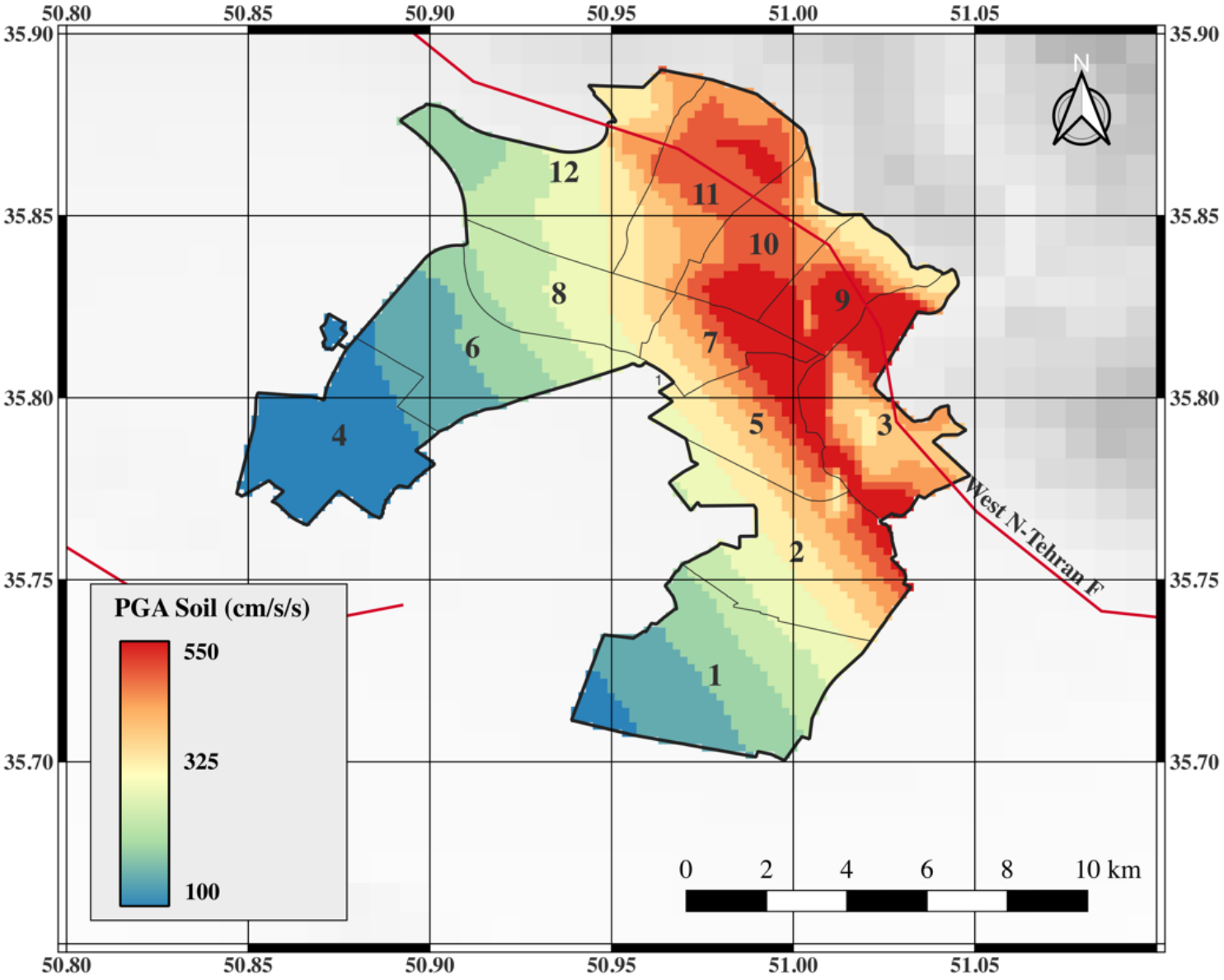

Figure 8

Distribution of PGA values on the soil surface in Karaj using NGA-west2 GMPEs

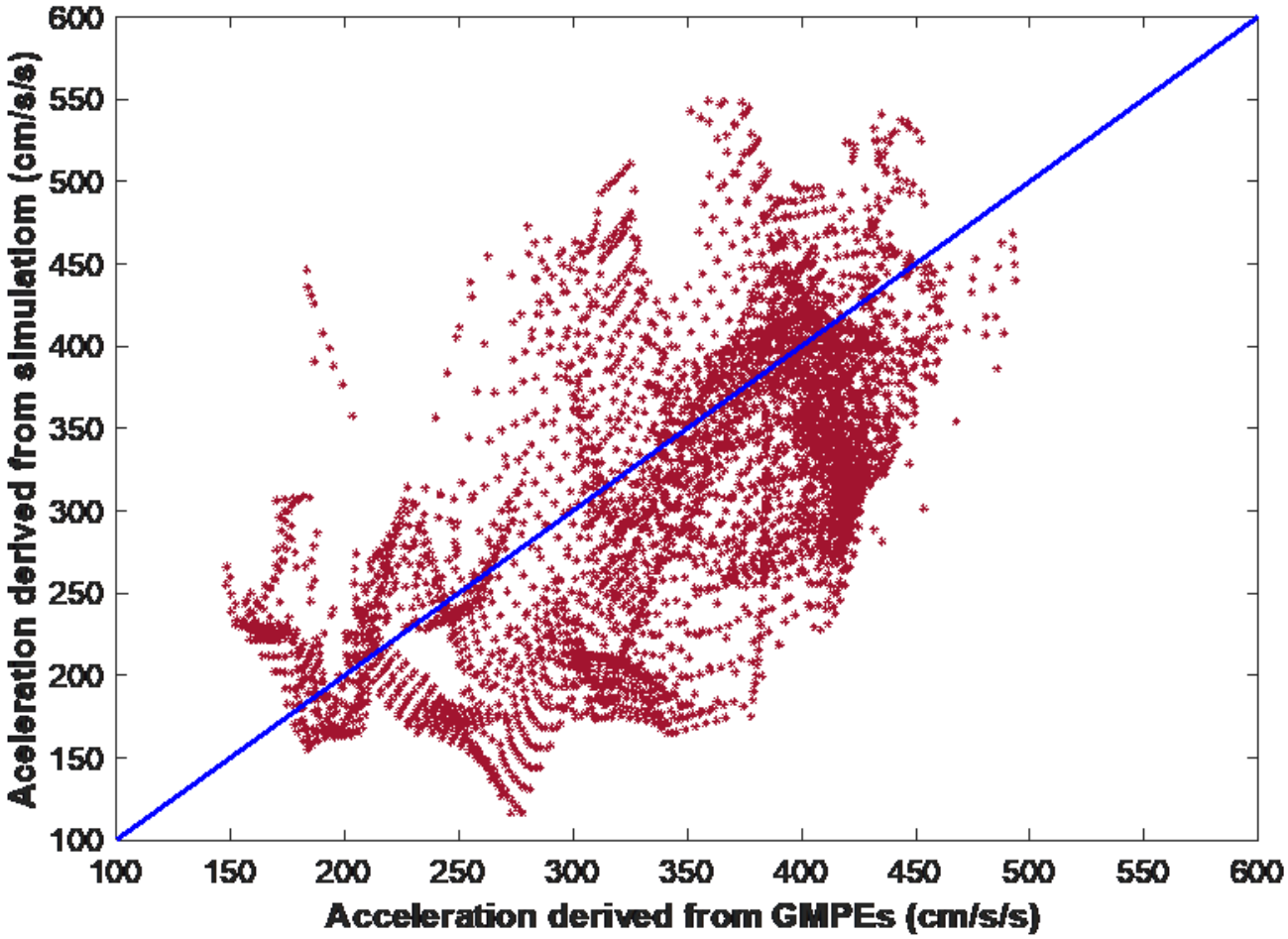

Figure 9

A grid-by-grid comparison of PGA values obtained from GMPEs and simulation

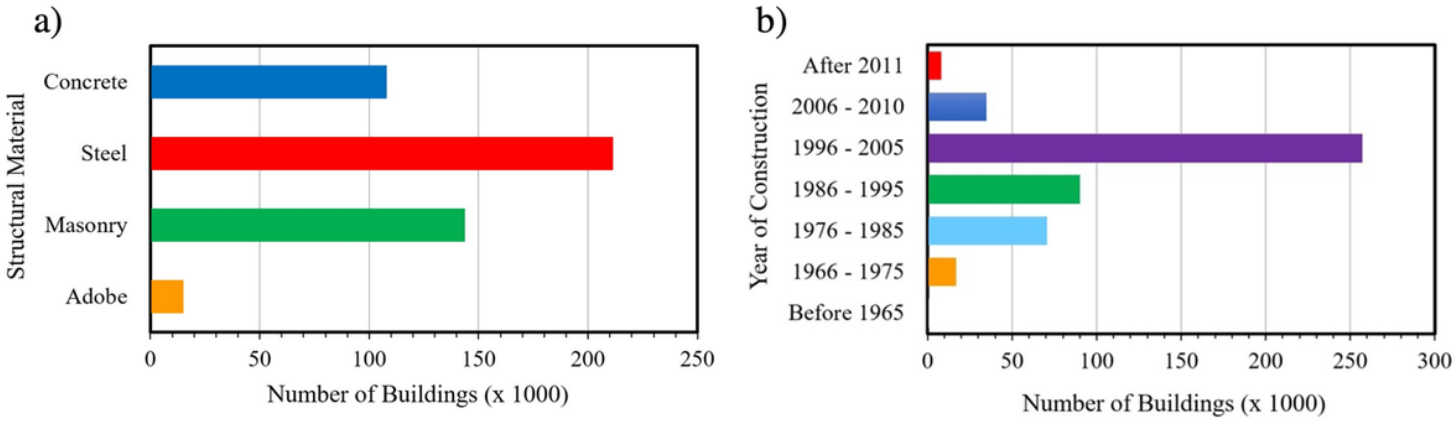

Figure 10

The number of buildings constructed a) using different construction material, b) in different years

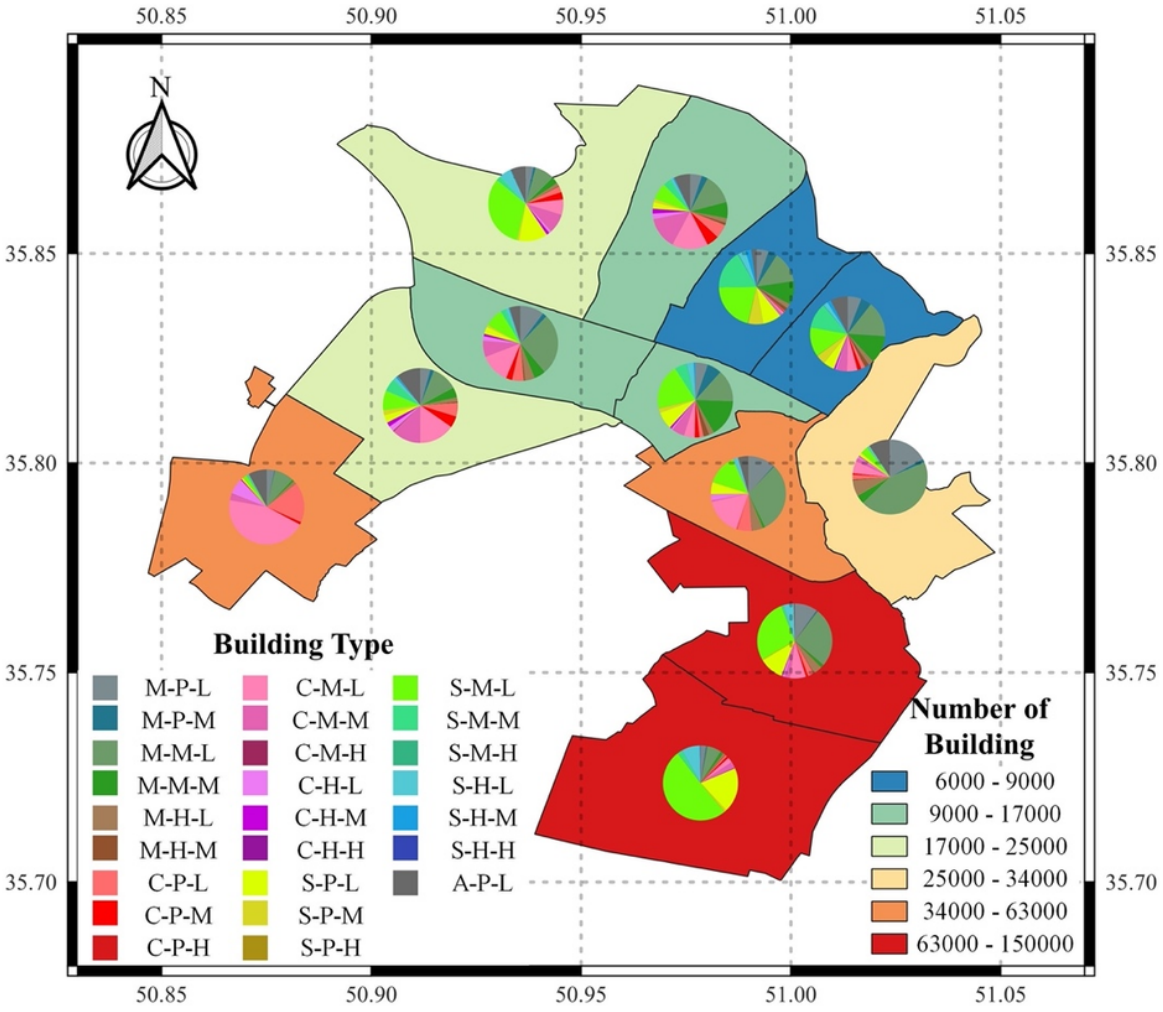

Figure 11

Distribution of different building classes within 12 municipal districts of Karaj

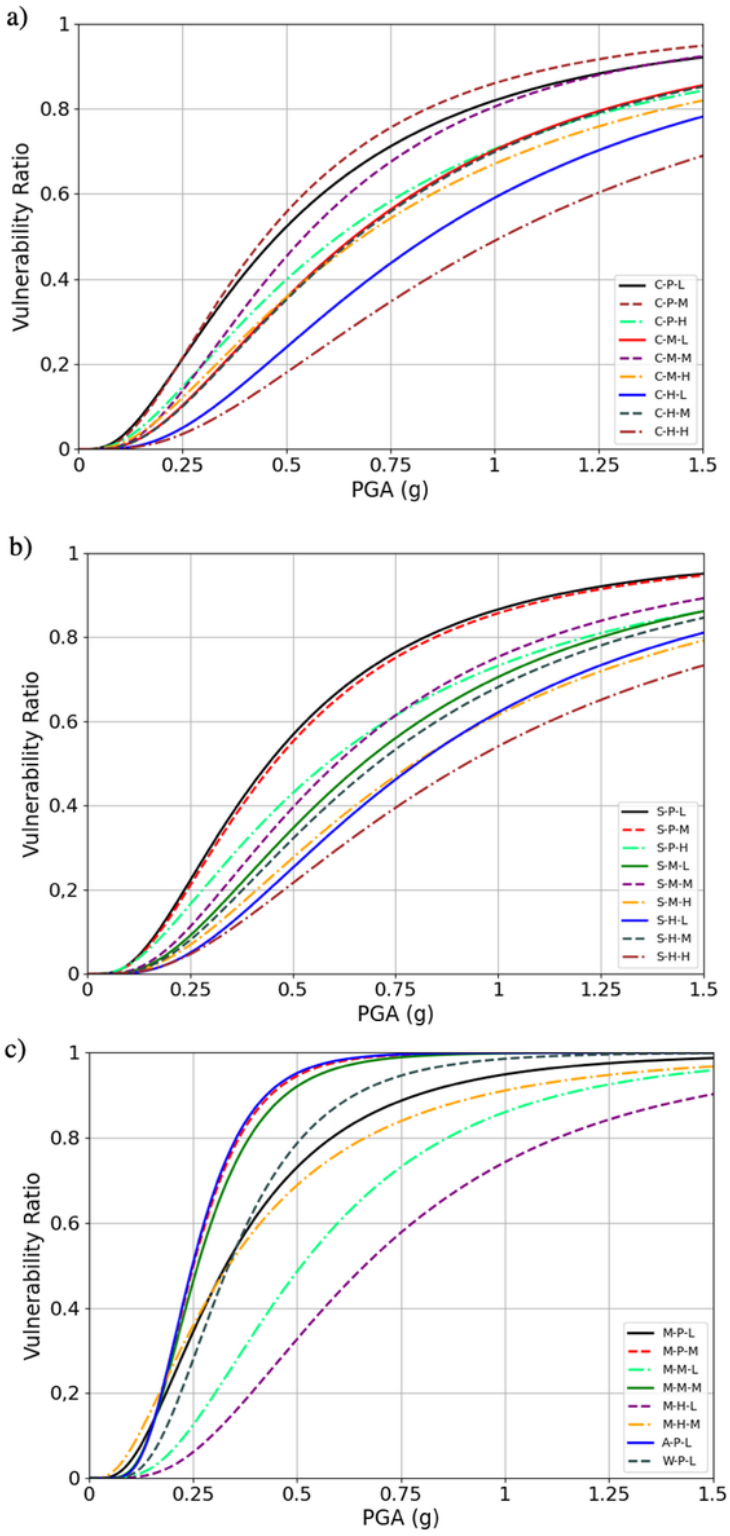

Figure 12

The vulnerability curves of Bastami et al (2022) for 26 building types

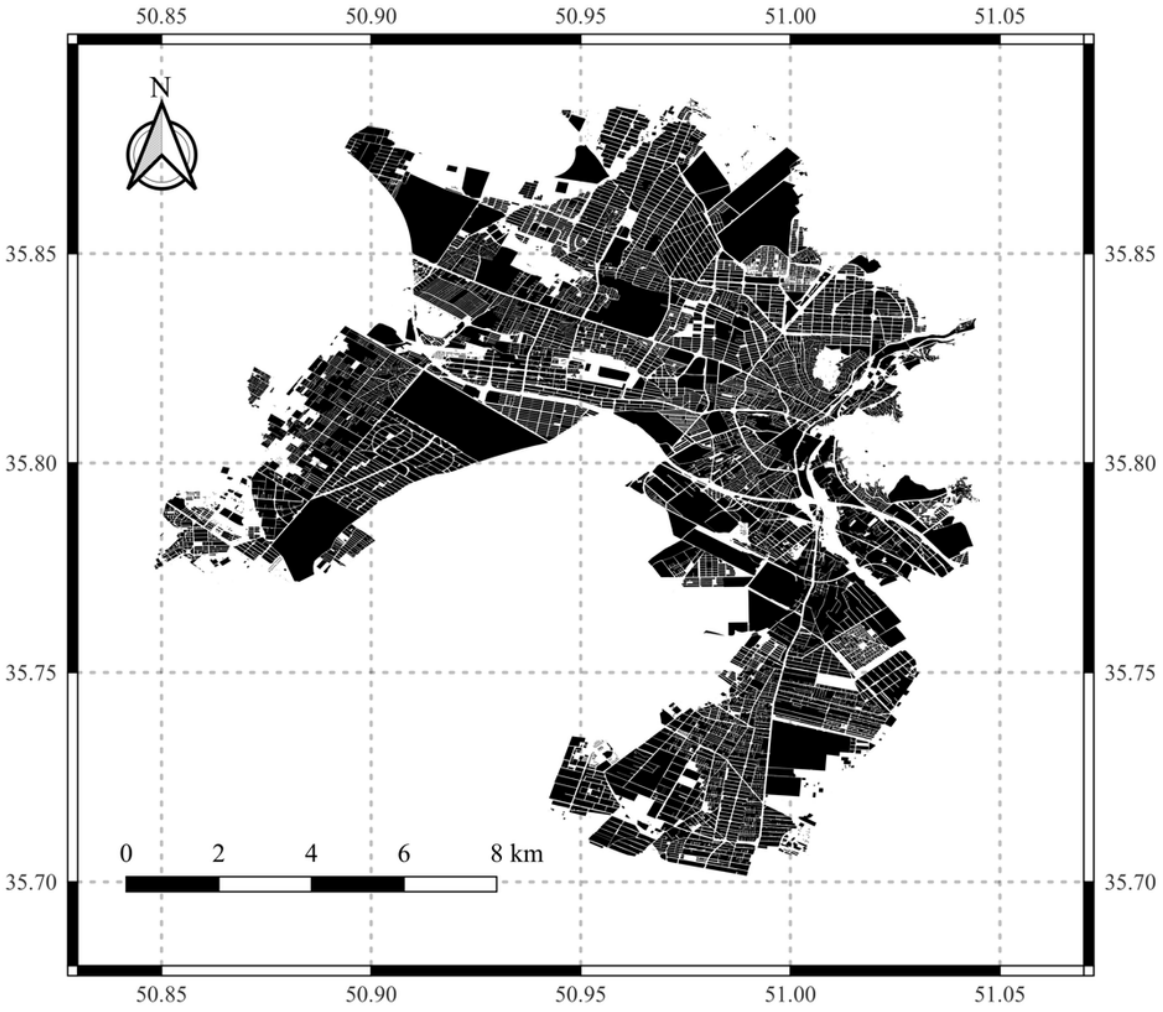

Figure 13

Distribution of census blocks within Karaj

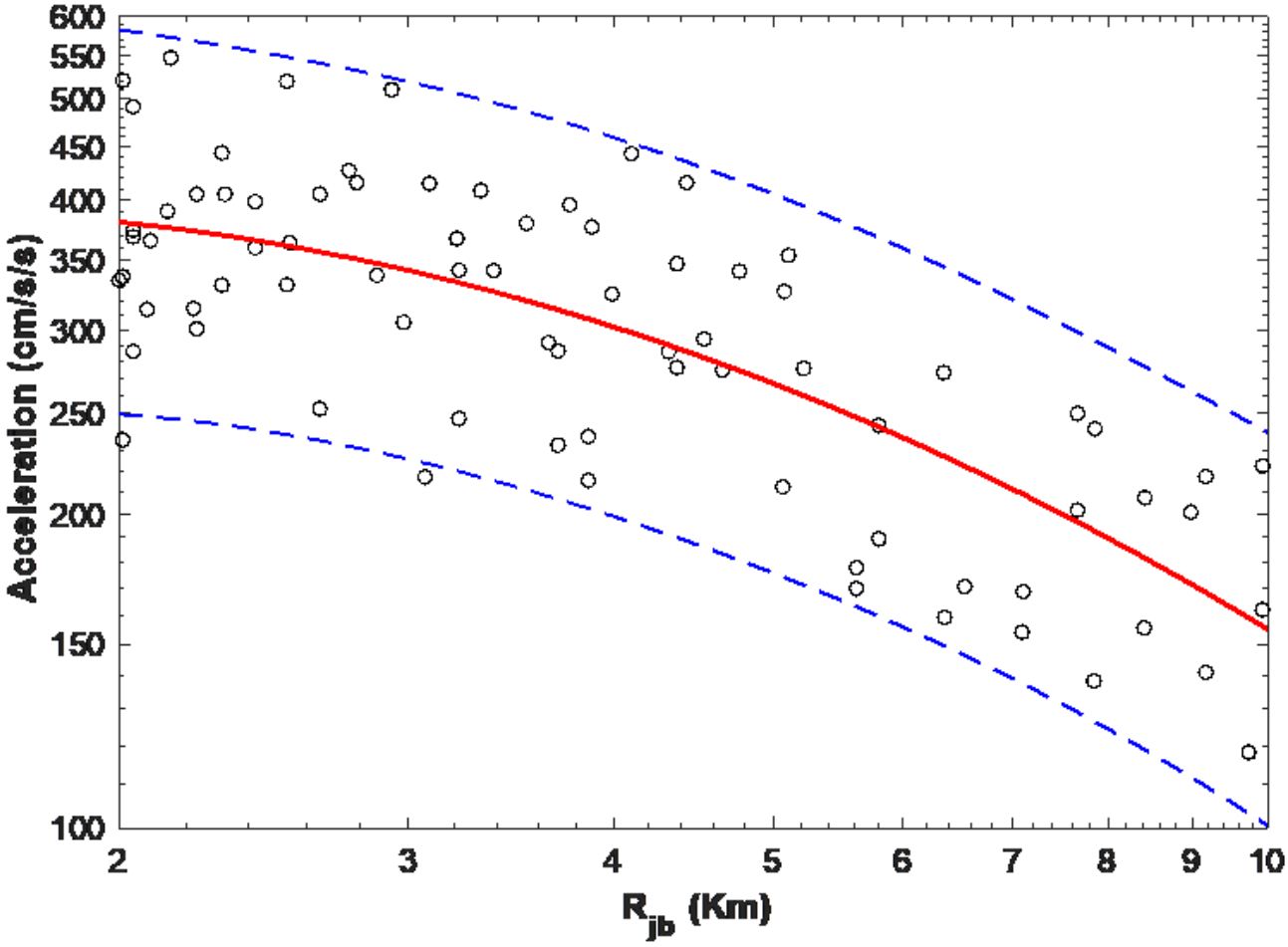

Figure 14

Distribution of PGA values from stochastic finite-fault approach in different grid cells

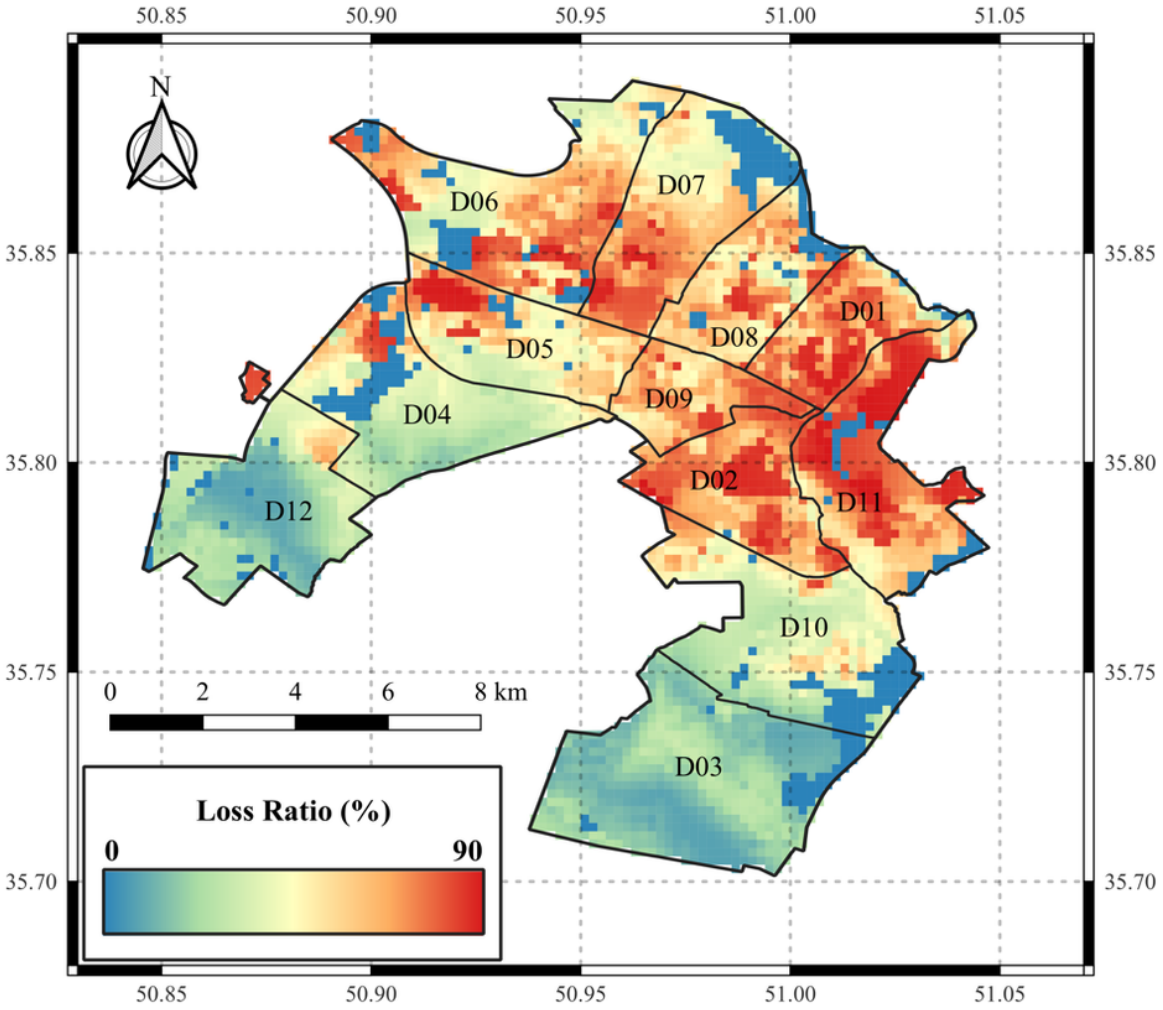

Figure 15

Distribution of loss ratio within 12 municipal districts of Karaj

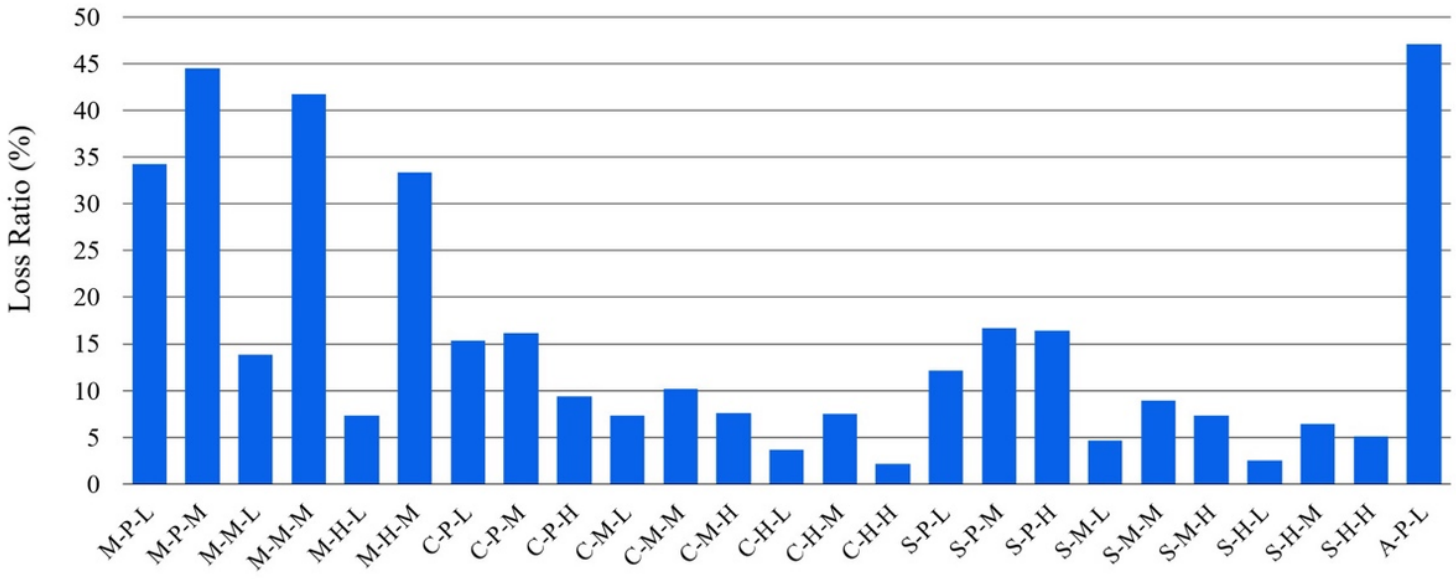

Figure 16

The loss ratio in different building types for the whole of Karaj

Supplementary Files

This is a list of supplementary files associated with this preprint. Click to download.

- Tables.docx